

## Coupling of evanescent and propagating guided modes in locally resonant phononic crystals

This content has been downloaded from IOPscience. Please scroll down to see the full text.

2014 J. Phys. D: Appl. Phys. 47 475502

(<http://iopscience.iop.org/0022-3727/47/47/475502>)

View [the table of contents for this issue](#), or go to the [journal homepage](#) for more

Download details:

IP Address: 193.140.240.110

This content was downloaded on 05/11/2014 at 14:59

Please note that [terms and conditions apply](#).

# Coupling of evanescent and propagating guided modes in locally resonant phononic crystals

Yan-Feng Wang<sup>1,2</sup>, Vincent Laude<sup>2</sup> and Yue-Sheng Wang<sup>1</sup>

<sup>1</sup> Institute of Engineering Mechanics, Beijing Jiaotong University, Beijing 100044, People's Republic of China

<sup>2</sup> Franche-Comté Electronique Mécanique Thermique et Optique, CNRS UMR 6174, Université de Franche-Comté, Besançon, France

E-mail: [vincent.laude@femto-st.fr](mailto:vincent.laude@femto-st.fr)

Received 28 July 2014, revised 24 September 2014

Accepted for publication 6 October 2014

Published 5 November 2014

## Abstract

In this paper, we present a combined theoretical, numerical and experimental study of acoustic wave propagation in 1D locally resonant phononic crystals made of acoustic resonators grafted onto a waveguide. The case of one single resonator grafted onto the waveguide is first investigated and a model of transmission cancellation at resonant frequencies is obtained. The model includes the excitation of evanescent guided waves attached to the grafting points. When extended to periodical arrays of grafted resonators, the model provides us with a definite theoretical expression for the complex band structure. Comparison with experimental results and complex band structures obtained by numerical simulation suggests a strong dependence of transmission through the crystal on the lattice constant of the grafted resonators. It is found that evanescent waves in the waveguide play a key role when the lattice constant is in the sub-wavelength range.

Keywords: phononic crystal, sonic crystal, metamaterial, local resonance

(Some figures may appear in colour only in the online journal)

## 1. Introduction

It is now well understood that band gaps in phononic crystals can arise both because of Bragg interference [1] or because of the presence of local resonances in the unit cell [2]. Since the propagation of waves is fully prohibited within band gaps, they appear as transmission dips in experiments. Considering the transmission properties through finite phononic crystals thus does not immediately inform on the exact mechanism which led to band gap formation. Relying on the band structure only is also not sufficient, as band gaps are characterized by an absence of any band rather than by a definite signature. The underlying physical mechanisms of Bragg and locally resonant (LR) band gaps, however, remain quite different. In the case of Bragg interference, the distribution of material in the crystal is heterogeneous and impedance variations (at interfaces between the inclusions and the matrix, for

example) are spatially distributed in the unit cell. For given materials composing the crystal, the frequency range of Bragg band gaps is mainly conditioned by the lattice constant. In the case of a local resonance, in contrast, waves propagating in a continuum matrix are coupled to the resonances of an array of resonators [3–6]. This coupling is ideally considered to be perfectly localized in space, i.e. to be described by a Dirac delta function. The resonant frequency is also relatively independent of the lattice constant, because band gaps appear in the continuum around the natural frequencies of the isolated resonator. LR phononic crystals are often advocated to lead to low-frequency or sub-wavelength band gaps, because of this independence with the lattice constant, while Bragg band gaps require comparatively longer lattice constants for the same result.

There is thus interest in identifying which of the two mechanisms, Bragg or local resonance, is at play for a given band



**Figure 1.** Photograph of one of the 1D phononic crystal samples. The 2 m long tube has a diameter of 10 cm.

gap, but also in clarifying the dependence of LR band gaps with the lattice constant, especially as the latter becomes small. We suggest in this paper that the complex band structure is an adequate theoretical tool for this purpose and that it can be compared to transmission experiments. In order to clarify the presentation of our ideas, but also to obtain a tractable model that can be later generalized to more complicated structures, we have chosen to study one of the simplest phononic crystals. We specifically study acoustic wave propagation in the audible frequency range through a one-dimensional (1D) phononic crystal consisting of a cylindrical polyvinyl chloride (PVC) tube with periodically grafted resonators, which conceptually approaches the phononic crystal with both linear defect (waveguide) and point defects (resonators) [3]. Different resonators and different lattice constants are considered in our experiments. Similar structures were already considered both theoretically and experimentally [7, 8]. The model that we propose, however, explicitly considers evanescent waves attached at the grafting points and extending inside the waveguide, a feature that was not introduced previously. This model is first constructed for the case of a single resonator and is then extended to include periodicity. The explicit expression of the complex band structure that results directly allows us to highlight differences between Bragg and LR band gaps. Comparison with experiment is satisfactory for both the single resonator and for the long-lattice periodical cases. For sub-wavelength lattice constants, a deterioration of band gaps is observed, that we attribute to interference between resonators.

## 2. Experiments with single grafted resonators

Figure 1 shows a photograph of one of the 1D phononic crystal samples. It is constructed on a PVC tube with an inner radius  $R = 5$  cm and a 2 mm thick wall. The tube is a waveguide for pressure acoustic waves in air. Only single-mode sound waves can propagate in this waveguide for frequencies between 0 and 2009 Hz [9]. For frequencies above 2009 Hz, propagation becomes multi-modal, a situation that we will not consider in the following. Periodic resonators in the form of PVC

tubes with a smaller diameter and closed at their extremity are grafted onto the waveguide with a period of either 8 or 25 cm. The radius of the resonators is 2.5 cm, and their length is either 24 cm for long resonators or 4 cm for short resonators. Such cylindrical resonators have a series of natural resonances whose frequencies are directly related to the tube length. The fundamental mode for a completely closed tube appears at the zero frequency; the same tube forms a Helmholtz resonator when connected to the waveguide [10].

Gaussian pulses with different central frequencies and bandwidths are generated with a simple sound card in a personal computer and played with a loudspeaker. The signals recorded with a microphone are sampled using the same sound card. The sampling rate of 384 kHz is amply sufficient to capture the relevant spectrum.

Before moving to 1D phononic crystal, we first considered a single resonator grafted on the waveguide, as sketched in figure 2. As a control experiment, the measurement of sound transmission through the bare tube is first presented in figure 3, where the wave source is a Gaussian pulse with a central frequency of 330 Hz. A transmission spectrum with a Gaussian shape would naively be expected, as propagation in the tube is monomodal and dispersionless with velocity  $c = 343$  m s<sup>-1</sup> (the celerity of pressure waves in open air under standard temperature and pressure conditions). However, Fabry–Perot oscillations [11] are observed, which are due to reflections at both ends of the 2 m long waveguide. The fitting line to the measured spectrum also indicates that the central frequency is shifted to around 280 Hz. This shift is possibly caused by frequency-dependent conversion efficiency at the entrance and exit of the waveguide. In the following, all experimental results are normalized against the measurement with the bare tube obtained with the same Gaussian short pulse. It should be noted that this normalization only smoothens the Fabry–Perot oscillations in the transmission but does not cancel them.

It was observed by Richoux *et al* that, for Helmholtz resonators, transmission spectra around the Helmholtz band gap are very sensitive to the incident signal amplitude [7]. This nonlinearity was explained by taking into account the quadratic term in the restoring force exerted on the air moving

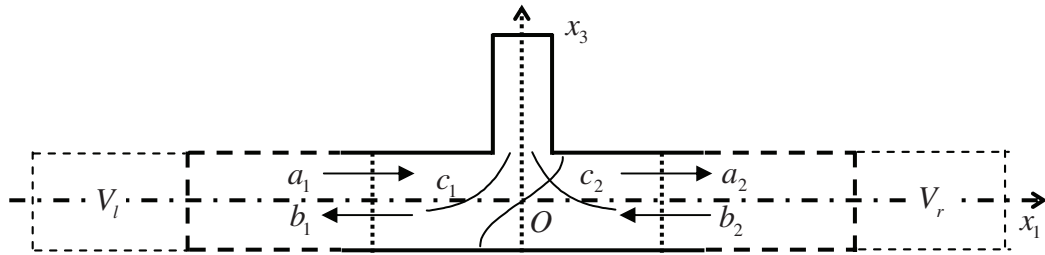


**Figure 2.** Sketch of a single resonator grafted onto a waveguide with a circular section.  $a_1$  and  $b_1$  ( $a_2$  and  $b_2$ , respectively) are the modal amplitudes of the propagating guided mode to the left (right, respectively) of the resonator.  $c_1$  ( $c_2$ , respectively) are the modal amplitudes of the first evanescent guided mode decaying toward the left (right, respectively) of the resonator. The additional parts indicated by thin-dashed lines and marked as  $V_l$  and  $V_r$  are waveguide regions used in the numerical calculation of the transmission.

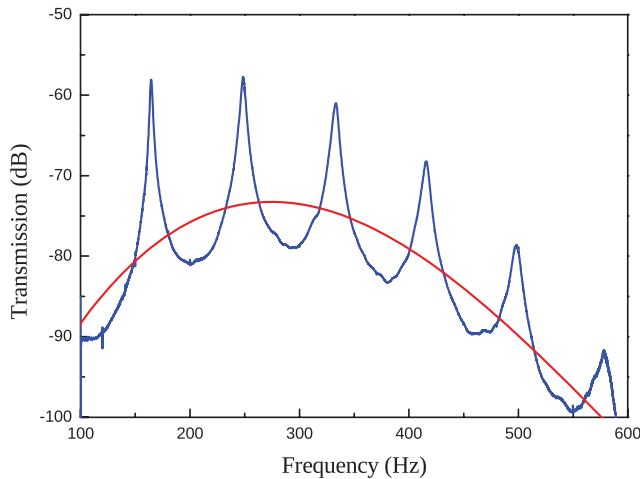


**Figure 3.** Experimental transmission through a bare tube (solid blue line) showing the Fabry-Perot oscillations caused by reflections at both ends of the waveguide. The solid red line is a fit with oscillations removed and serves to indicate the spectral contents of the measurement.

within the neck of the resonator. We note that there is no small neck in our samples. The nonlinearity is negligible in our samples, which we verified by repeating our experiments at different signal levels.

Experimental results for single resonators are presented in figure 4. For comparison, numerically simulated results are also presented (a mass density  $\rho = 1.2041 \text{ kg m}^{-3}$  and a velocity  $c = 343 \text{ m s}^{-1}$  are used for air in all of our numerical simulations). In order to evaluate numerically the transmission of our samples, we used a time-harmonic finite element model (FEM) of pressure wave propagation. In addition to the geometry of the sample, two additional one-wavelength long regions (marked as  $V_l$  and  $V_r$  in figure 3) are added to the structure. A radiation boundary condition including an incident harmonic plane wave with unit amplitude is imposed on the left boundary, and a simple radiation boundary condition is used on the right boundary. With this setting, reflections at the ends of the waveguide are avoided so the Fabry-Perot oscillations do not appear in the simulated spectra. Transmission can be evaluated after the pressure field  $p$  inside the waveguide has been obtained numerically as  $t = \int p e^{ikx} dV_r / \int p e^{ikx} dV_l$ .

It can be noticed that the transmissions in figure 4 vary with different resonators and different resonant frequencies

of the same resonator. Transmission dips appear clearly around 1459.7 Hz for the short resonator, and around 335.6, 1000.0, and 1645.8 Hz for the long resonator. The simulated and experimental results agree reasonably well with each other. Simulated pressure distributions at the frequency of the dips are shown as insets in figure 4. Clearly, the pressure field is localized inside the resonators. The modal distribution of these local resonances look very much like the  $n$ th ( $n = 0, 1, 2$ ) order natural vibration modes of the resonator. The natural frequencies of the isolated resonator with two closed ends and length  $l$  are given by  $\Omega_n / (2\pi) = nc / (2l)$ , and they are clearly different from the resonant frequencies obtained from transmission dips, see table 1. In general, the phenomenon of transmission cancelling appears at a resonant frequency that is different from the natural frequency. In the following section this property is explained by the excitation of evanescent guided waves attached to the grafting point.

### 3. Model of local resonance

In this section, a theoretical model is developed to explain the transmission cancelling and frequency shift. Let us consider a cylindrical waveguide supporting only one fundamental propagating mode for angular frequencies  $\omega < 1.84c/R$ , with  $R$  the radius of the waveguide [9]. As depicted in figure 2, a resonator is grafted to the side of the waveguide. For our purpose, we will not need to explicit precisely the details of the resonator. Its resonant behaviour can be simply understood by stating that even a vanishingly small excitation can set it into motion, providing it is applied with the correct frequency. A model of this behaviour is the forced harmonic oscillator with equation

$$Cu + M \frac{\partial^2 u}{\partial t^2} = F e^{i\omega t} \quad (1)$$

with  $M$  being a mass,  $C$  a stiffness, and  $F$  a force.  $u$  here represents the displacement of the centre of the mass with respect to an equilibrium position. The same simple model is found with optical or electrical resonators, for instance, with a different physical meaning attached to the parameters of the model (i.e. dielectric constant, or capacitance and inductance). Under harmonic motion,  $u = \bar{u} e^{i\omega t}$ , and the resonator equation becomes

$$(C - \omega^2 M) \bar{u} = F \quad (2)$$

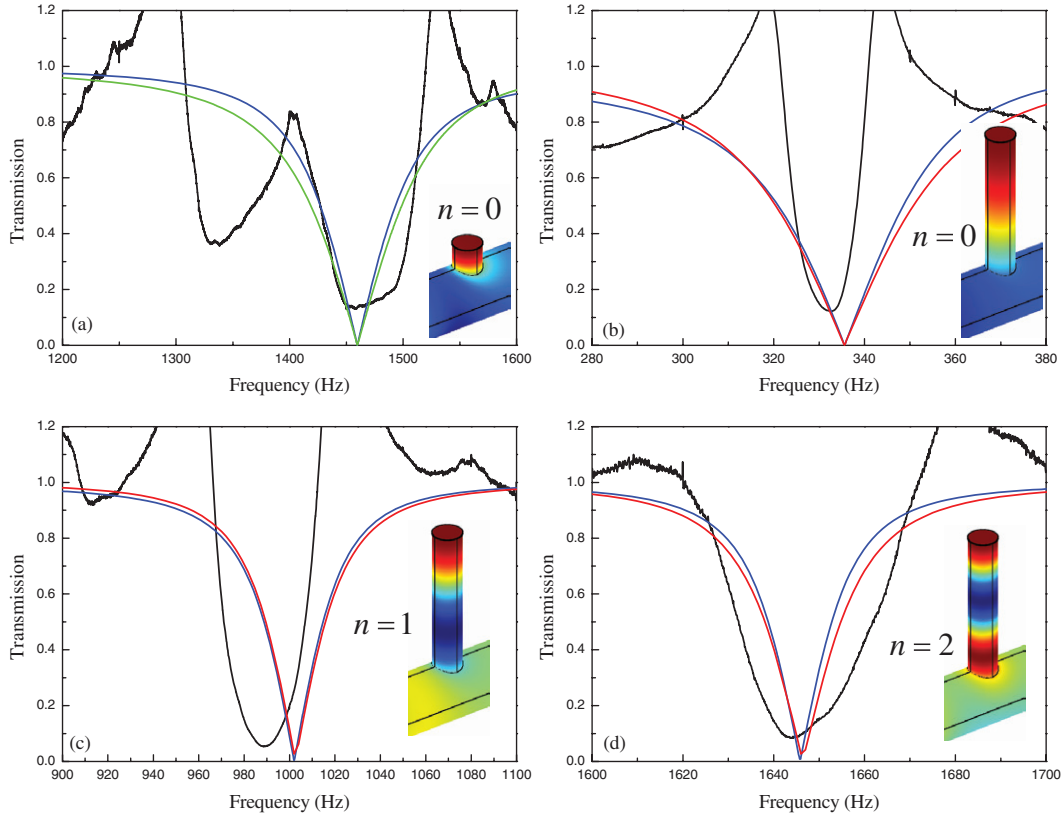


**Figure 4.** Transmission of a single (a) short and (b)–(d) long resonator grafted onto the waveguide. Panels (b)–(d) show the transmission at frequencies related to the 0th, 1st and 2nd acoustic resonance of the single long resonator, respectively. The insets show the vibration modes at the resonant frequency obtained from a FEM simulation. The black, blue and green lines represent the experimental, theoretical and simulated results, respectively.

**Table 1.** Natural frequencies  $\Omega_n/(2\pi) = nc/(2l)$  and resonant frequencies  $\omega_0(2\pi)$  of resonators grafted onto the waveguide. Coupling coefficient values are obtained from a fit to the single resonator transmission.

Resonator parameters	$l = 4\text{ cm}$		$l = 24\text{ cm}$	
	$n = 0$	$n = 0$	$n = 1$	$n = 2$
$\Omega_n/(2\pi) = nc/(2l)$ (Hz)	0	0	714.6	1429.2
$\omega_0(2\pi)$ (Hz)	1459.7	335.6	1000.0	1645.8
$\kappa_{11}$ ( $\text{rad}^2\text{m}^{-1}\text{s}^{-2}$ )	$1.6 \times 10^8$	$7.6 \times 10^6$	$6.0 \times 10^7$	$7.1 \times 10^7$
$\kappa_{12}$ ( $\text{rad}^2\text{m}^{-1}\text{s}^{-2}$ )	$8.1 \times 10^8$	$5.0 \times 10^6$	$2.7 \times 10^7$	$2.8 \times 10^7$
$K_{22}$ ( $\text{rad}^2\text{m}^{-1}\text{s}^{-2}$ )	$4.3 \times 10^9$	$3.2 \times 10^8$	$1.2 \times 10^9$	$1.1 \times 10^9$

with  $\Omega = \sqrt{C/M}$  being the natural frequency. The oscillation amplitude  $\bar{u}$  has the Lorentzian frequency dependence

$$\bar{u} = \frac{F/M}{\Omega^2 - \omega^2} = \frac{F}{M}L(\omega). \quad (3)$$

Obviously,  $\bar{u}$  becomes infinite at the resonance condition  $\omega = \Omega$ .

Now, we wish to describe the interaction of the waveguide with the resonator, and ultimately to compute a reflection and a transmission for waves inside the waveguide. As the waveguide is monomode, the pressure field far from the resonator can be written as the superposition

$$p_1(\mathbf{x}) = \begin{cases} \psi_1(x_2, x_3)(a_1e^{-i\beta x_1} + b_1e^{+i\beta x_1}) & \text{if } x_1 < 0 \\ \psi_1(x_2, x_3)(a_2e^{-i\beta x_1} + b_2e^{+i\beta x_1}) & \text{if } x_1 > 0 \end{cases} \quad (4)$$

with wavenumber  $\beta = \omega/c$ . The guided mode is thus a propagation channel for waves travelling to the right and to the left with complex amplitudes  $a_i$  and  $b_i$ .  $\psi_1(x_2, x_3)$  is the modal transverse distribution.

In close proximity of the resonator, the situation is different. Far from the connection between waveguide and resonator, the force density is identically zero at equilibrium. In the vicinity of the connection, however, the boundary conditions are modified and the field inside the waveguide induces a force that can drive the resonator. Accordingly, energy from the waveguide will be dragged by the resonator and will set it into motion. Reciprocally, the motion of the resonator acts back on the waveguide and changes its equilibrium very locally. As a useful idealization, we will consider that the connection can be reduced to a single point at  $x_1 = 0$  where the force density is proportional to a Dirac delta function  $\delta(x_1)$ . Such a localized

excitation of the waveguide results in the excitation of bound modes composed of evanescent waves [12]. There are in principle infinitely many evanescent waves in the waveguide [13]. For simplicity, we will only retain the dominant evanescent guided mode with imaginary part of the wavenumber given by  $\alpha = \sqrt{(1.84/R)^2 - (\omega/c)^2}$ . There is thus a second channel for transmission through the waveguide, centred on the connection point and such that

$$p_2(\mathbf{x}) = \begin{cases} c_1\psi_2(x_2, x_3)e^{\alpha x_1} & \text{if } x_1 < 0 \\ c_2\psi_2(x_2, x_3)e^{-\alpha x_1} & \text{if } x_1 > 0 \end{cases} \quad (5)$$

where  $\psi_2(x_2, x_3)$  is the modal transverse distribution for the evanescent guided mode. The appearance of evanescent waves inside the waveguide can be understood as arising from the Green's function of the waveguide under the excitation  $\delta(x_1)$ .

At any position along the waveguide, except at exactly  $x_1 = 0$ , the total field is the superposition  $p(\mathbf{x}) = p_1(\mathbf{x}) + p_2(\mathbf{x})$ . At the connection point, we will assume that the field  $p$  is continuous. Because the modes are mutually orthogonal, the following two conditions should be satisfied,

$$a_1 + b_1 = a_2 + b_2 \text{ and } c_1 = c_2. \quad (6)$$

If the field  $p$  is continuous at the junction, its first derivative  $\partial p / \partial x_1$  is not. Actually,  $\partial p_2 / \partial x_1$  for  $p_2$  given by equation (5) is clearly discontinuous, and so should the superposition be. We write the jump of  $\partial p / \partial x_1$  as

$$\left[ \frac{\partial p}{\partial x_1} \right]_{0^-}^{0^+} = L(\omega)\kappa(x_2, x_3)p(0, x_2, x_3), \quad (7)$$

which can be obtained by integration of the wave equation in the waveguide subject to a force density  $L(\omega)\kappa(x_2, x_3)p(\mathbf{x})\delta(x_1)$ , meaning that the resonator was initially set into motion by the field distribution  $p(\mathbf{x})$  at the junction, with a resonant line shape given by the Lorentzian line shape  $L(\omega)$ , and creates back a stress distribution with some cross-section dependence indicated by  $\kappa(x_2, x_3)$ , which is a function of  $x_2$  and  $x_3$ . Projecting equation (7) on the two modes, we obtain a pair of equations

$$i\beta(-a_2 + b_2) - i\beta(-a_1 + b_1) = L(\omega)(\kappa_{11}(a_1 + b_1) + \kappa_{12}c_2) \quad (8a)$$

and

$$-\alpha(c_1 + c_2) = L(\omega)(\kappa_{21}(a_1 + b_1) + \kappa_{22}c_2) \quad (8b)$$

with  $\kappa_{ij} = \int \kappa(x_2, x_3)\psi_i(x_2, x_3)\psi_j(x_2, x_3)dx_2dx_3$ .

The presence of the discontinuity thus acts as a mixer of the two types of modes, which are otherwise completely uncoupled along the waveguide.

We define next the coefficients  $\gamma_{1j} = L(\omega)\kappa_{1j}/(2i\beta)$  and  $\gamma_{2j} = L(\omega)\kappa_{2j}/(2\alpha)$ . The equation system relating outgoing amplitudes ( $a_2$  and  $b_1$ ) to incoming amplitudes ( $a_1$  and  $b_2$ ) can then be written as the scattering matrix

$$\begin{pmatrix} 1 & -1 & 0 \\ 1/2 & 1/2 + \gamma_{11} & \gamma_{12} \\ 0 & \gamma_{21} & 1 + \gamma_{22} \end{pmatrix} \begin{pmatrix} a_2 \\ b_1 \\ c_2 \end{pmatrix} = \begin{pmatrix} 1 & -1 \\ 1/2 - \gamma_{11} & 1/2 \\ -\gamma_{21} & 0 \end{pmatrix} \begin{pmatrix} a_1 \\ b_2 \end{pmatrix}. \quad (9)$$

The solution to this linear system can be obtained exactly as

$$\begin{pmatrix} a_2 \\ b_1 \\ c_2 \end{pmatrix} = \begin{pmatrix} t & r \\ r & t \\ s & s \end{pmatrix} \begin{pmatrix} a_1 \\ b_2 \end{pmatrix} \quad (10)$$

with

$$t = (1 + \gamma_{22})/D, r = t - 1, \text{ and } s = -\gamma_{21}/D, \quad (11)$$

where  $D = (1 + \gamma_{11})(1 + \gamma_{22}) - \gamma_{12}\gamma_{21}$ ,  $r$  and  $t$  have the meaning of a reflection coefficient and of a transmission coefficient, respectively.  $s$  measures the part of the incoming amplitudes that are stored in the evanescent wave. For frequencies far from resonance, the  $\gamma_{ij}$  coefficients are negligible and it follows that  $t = 1$ , i.e. waves are simply transmitted through the waveguide without reflection and significant excitation of the resonator.  $r$  and  $t$  are generally seen to be related by the simple formula  $r = t - 1$ , implying that if the transmission vanishes, then the incident wave is fully reflected (with a phase shift of  $\pi$ ). The condition for  $t = 0$  is given by  $1 + \gamma_{22} = 0$ , which can happen at the resonant frequency

$$\omega_0^2 = \Omega^2 + \frac{\kappa_{22}}{2\alpha}. \quad (12)$$

Transmission cancelling thus occurs mostly thanks to the Lorentzian line shape: even if the coupling strength is small, the undamped resonator will be able to cancel exactly the transmission through the waveguide at a frequency close to but different from the natural frequency  $\Omega$ . It can be seen that this simple model predicts that the shift of the resonant frequency compared to the natural frequency of the resonator, as shown in table 1, is due to the excitation of evanescent guided modes.

The transmissions predicted by (11) and (12) are also presented in figure 4, with the fitting parameters  $\kappa_{11}$ ,  $\kappa_{12}(=\kappa_{21})$  and  $\kappa_{22}$  being listed in table 1. A very good agreement is found between the model and numerical simulations, meaning that the model captures most of the important features of transmission cancelling. The transmission curves in the experiment seem more rounded than those obtained from simulation and theory, which we attribute to losses that are present in the experiment but that are not taken into account by either the finite element analysis or the simplified model.

#### 4. Experiments with periodically grafted resonators

Next we consider periodic arrays of resonators grafted onto the waveguide. Experimental samples were prepared with five identical resonators each. Considering the two different resonator lengths ( $l = 4$  cm and 24 cm) and the two different lattice constants ( $a = 8$  and 25 cm), there are four different samples. In addition to the experimental results shown in figures 5 and 6, the complex band structures obtained by FEM are also displayed. To obtain the complex band structures, we substitute the Bloch-Floquet expression  $p = \bar{p}e^{i(\omega t - kx)}$  with  $\bar{p}$  being a periodic function of space into the acoustic wave equation  $\partial^2 p / \partial t^2 = c^2 \partial^2 p / \partial x^2$ . We then get the generalized wave equation

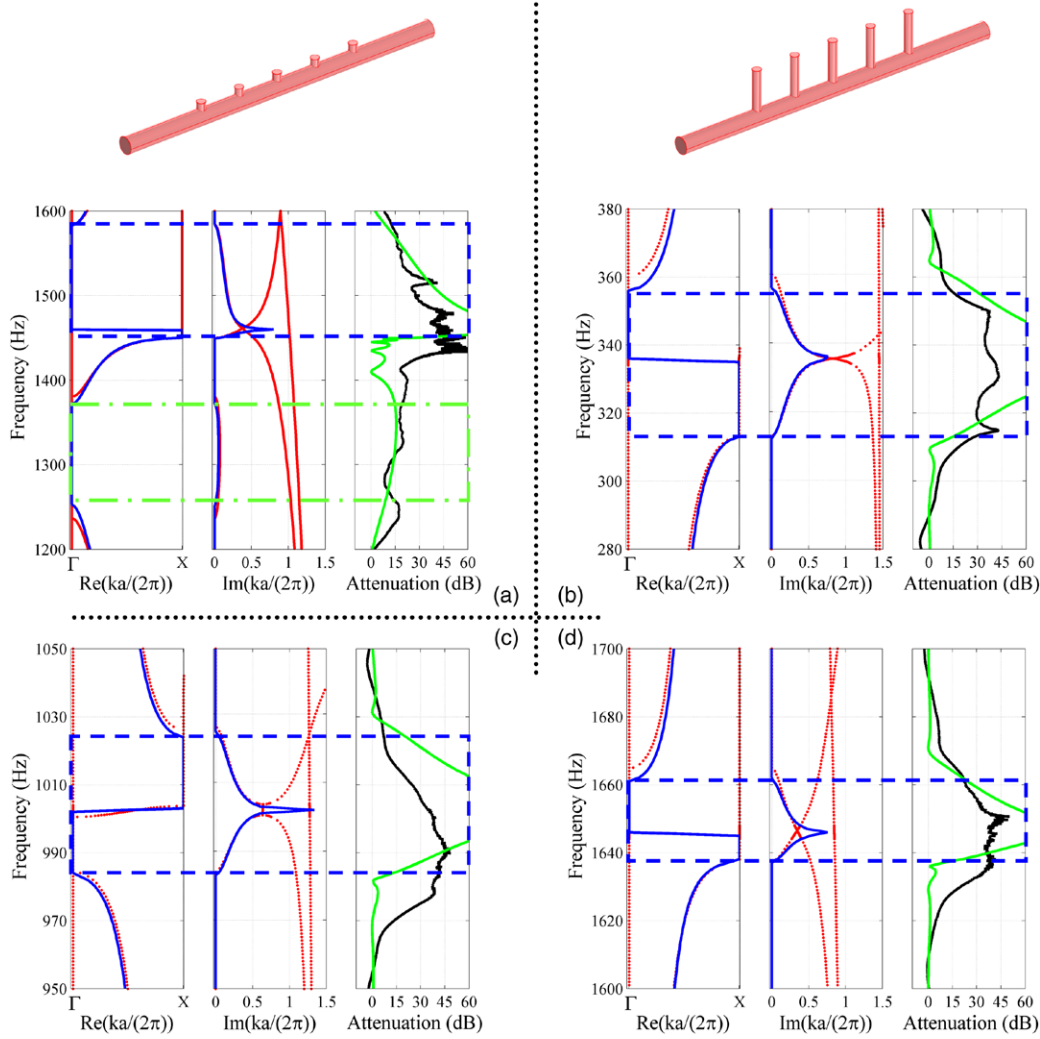


**Figure 5.** Complex band structures (real part on the left and imaginary part in the middle of each panel) and transmission properties (on the right of each panel) for 1D phonic crystals with a periodic array of (a) short and (b)–(d) long resonators (lattice constant  $a = 25$  cm). The blue and red lines in the complex band structures represent the theoretical and the numerical results, respectively. The black and green lines in the transmission spectra represent the experimental and numerical results, respectively. The blue dashed lines mark the LR band gap predicted by the theoretical model. The green dashed–dotted lines in panel (a) mark the Bragg band gap predicted by the theoretical model.

$$c^2 \left( \frac{\partial^2 \bar{p}}{\partial x_1^2} - 2ik \frac{\partial \bar{p}}{\partial x_1} - k^2 \bar{p} \right) + \omega^2 \bar{p} = 0. \quad (13)$$

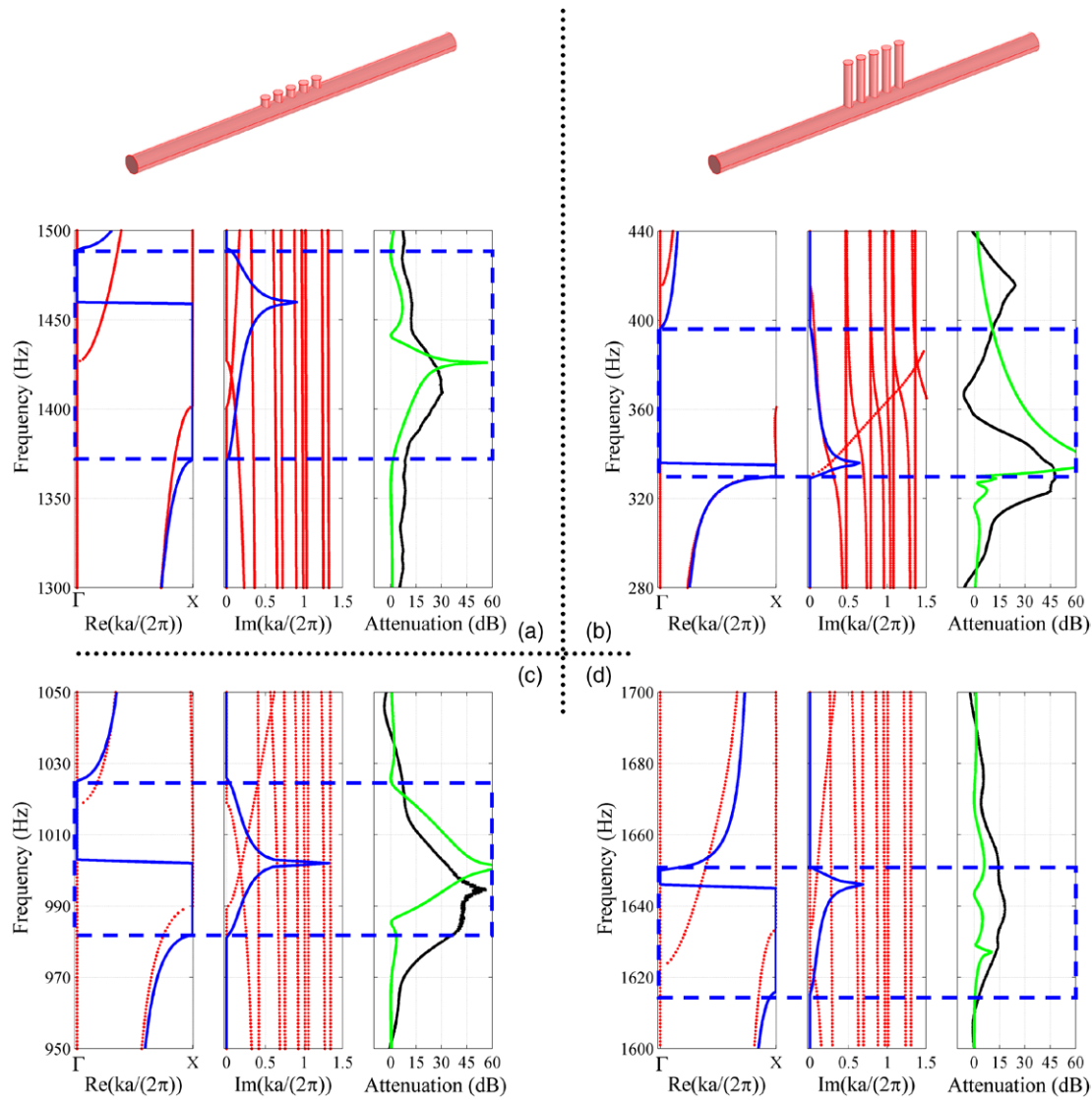
This equation is solved as a generalized eigenvalue problem for the wavenumber  $k$ . Neumann boundary conditions are imposed on all the boundaries, except for the left and the right boundaries, which are related by a periodic boundary condition. The complex band structures can be obtained by letting  $\omega$  sweep the frequency range of interest [14].

Figure 5 shows the results for the lattice constant  $a = 25$  cm. LR band gaps appear around the resonant frequencies previously found for the single resonators. They are comparatively broader than the transmission dips for the single resonator, in accordance with the complex band structures computed with FEM.

In the short resonator case, in figure 5(a), an additional Bragg band gap appears around 1372 Hz ( $\sim c/a$ ), just below the LR band gap. The attenuation inside the LR band gap is found to be larger than that inside the Bragg band gap. All these features can be clearly explained by the complex band structures.

The smallest imaginary part of the complex wavenumber for the LR band gap is larger than that of the Bragg band gap. As a result, a stronger attenuation is expected in the LR band gap as compared to the Bragg one. The complex band structure has a different shape within the Bragg and the LR band gaps. In the Bragg case, the band gap opens at the  $\Gamma$  point of the first Brillouin zone and the complex imaginary band connecting the entrance and the exit of the band gap is continuous and very smooth. In contrast, the entrance and the exit of the LR band gap occur at opposite symmetry points of the Brillouin zone and the complex imaginary band connecting them is composed of two crossing bands forming a cusp.

In the long resonator case, in figures 5(b)–(d), LR band gaps appear around the three different resonant frequencies under the cutoff frequency for the second guided mode of the waveguide. Bragg band gaps are not clearly observed in this case due to their small attenuation and to the disturbance caused by Fabry–Perot oscillations. Furthermore, there is no hybridization of the Bragg bandgap and of the LR bandgap



**Figure 6.** Complex band structures (real part on the left and imaginary part in the middle of each panel) and transmission properties (on the right of each panel) for 1D phononic crystals with a periodic array of (a) short and (b)–(d) long resonators (lattice constant  $a = 8$  cm). The blue and red lines in the complex band structures represent the theoretical and the numerical results, respectively. The black and green lines in the transmission spectra represent the experimental and numerical results, respectively. The blue dashed lines mark the LR band gap predicted by the theoretical model.

such as reported, e.g. in [15] and [16]. The complex band structure around the LR band gaps also has the features discussed above for the short resonator. It can also be remarked that inside the experimental LR band gaps, the transmission seems to be a combination of a series of dips. This may be due to the interference of guided waves trapped between the resonators and creating a super-modal structure of the series of five resonators [6].

Next, we consider similar phononic crystals but with the smaller lattice constant  $a = 8$  cm. Experimental and numerical results are shown in figure 6. For the short resonators, in figure 6(a), only one LR band gap exists around 1420 Hz. Compared to the resonant frequency of the single resonator or with the long lattice constant (see table 2), a small frequency shift thus appears. Since for this frequency the lattice constant is about three times smaller than the wavelength, we suggest that the frequency shift can be due to the interference of

guided waves reflecting at the resonators. The complex band structure obtained by FEM correctly predicts this frequency shift. Compared to figure 5(a), a smaller attenuation in the LR band gap is also found.

For the long resonators, in figures 6(b)–(d), three LR band gaps appear around the resonant frequencies. Compared to the long lattice constant case, the attenuation inside the first and the second LR band gaps do not change too much. For the third LR band gap, however, the attenuation is clearly much poorer. It is even smaller than the attenuation for the single resonator in figure 4(d). Strikingly, the third LR band gap is not even predicted anymore by the complex band structure. The appearance of the first two LR bands gaps is predicted but the frequency ranges do not match well with experiment. Interestingly, all three LR band gaps are still correctly predicted by the periodic model that we will introduce in the following section. The disagreement between experimental results and the complex

**Table 2.** Transmission cancelling frequencies (Hz) for single resonators and periodically grafted resonators.

Cases		l = 4 cm		l = 24 cm	
		n = 0	n = 0	n = 1	n = 2
Single resonator	Experiment	~1460	~333	~989	~1644
	Theory	1460	336	1000	1646
	Simulation	1460	336	1000	1646
Periodically grafted resonators (a = 25 cm)	Experiment	~1440	~330	~990	~1651
	Theory	1460	336	1002	1646
	Simulation	1460	336	1002	1646
Periodically grafted resonators (a = 8 cm)	Experiment	~1420	~330	~995	~1639
	Theory	1460	336	1002	1646
	Simulation	1424	335	1000	/

Note: The simulation results for the periodic case are obtained from the computed complex band structures.

band structure computed with FEM (see table 2) may be again attributed to the interference of resonators. For a finite array of five resonators, this interference remains limited. However, when we compute the complex band structure, an infinite array of resonators is considered. Interference becomes very significant, and can even close the LR band gap.

### 5. Periodic model of local resonance

In this section, the theoretical model of section 3 is further extended to provide an explicit formula of the complex band structure near a local resonance. We first rewrite the scattering matrix of equation (10), limited to the amplitudes of the propagating guided mode, as the transmission matrix

$$\begin{pmatrix} a_2 \\ b_2 \end{pmatrix} = \begin{pmatrix} \frac{t^2 - r^2}{t} & \frac{r}{t} \\ -\frac{r}{t} & \frac{1}{t} \end{pmatrix} \begin{pmatrix} a_1 \\ b_1 \end{pmatrix}. \quad (14)$$

It can be easily verified that the determinant of this transmission matrix is unity. We wish to relate the modal amplitudes at both ends of the unit-cell of the crystal. We thus use the propagators

$$\begin{pmatrix} a'_2 \\ b'_2 \end{pmatrix} = \begin{pmatrix} e^{-i\beta a/2} & 0 \\ 0 & e^{+i\beta a/2} \end{pmatrix} \begin{pmatrix} a_2 \\ b_2 \end{pmatrix} \quad (15a)$$

and

$$\begin{pmatrix} a'_1 \\ b'_1 \end{pmatrix} = \begin{pmatrix} e^{-i\beta a/2} & 0 \\ 0 & e^{+i\beta a/2} \end{pmatrix} \begin{pmatrix} a_1 \\ b_1 \end{pmatrix} \quad (15b)$$

to obtain

$$\begin{pmatrix} a'_2 \\ b'_2 \end{pmatrix} = \begin{pmatrix} \frac{t^2 - r^2}{t} e^{-i\beta a} & \frac{r}{t} \\ -\frac{r}{t} & \frac{1}{t} e^{+i\beta a} \end{pmatrix} \begin{pmatrix} a'_1 \\ b'_1 \end{pmatrix} = T \begin{pmatrix} a'_1 \\ b'_1 \end{pmatrix}. \quad (16)$$

We can now apply Bloch's theorem. As the problem is scalar, we can write Bloch waves as  $p_1(\mathbf{x}) = \bar{p}_1(\mathbf{x})e^{-ikx_1}$  with

$\bar{p}_1(\mathbf{x})$  being periodic. In particular, we have the periodic Bloch boundary conditions

$$p_1(a/2, x_2, x_3) = p_1(-a/2, x_2, x_3)e^{-ika}. \quad (17)$$

Such periodic boundary conditions are somehow weaker than the original Bloch's theorem, but are sufficient to determine the solution of the problem. Indeed, they show that  $\lambda = e^{-ika}$  is an eigenvalue of the transmission matrix  $T$ . In order to obtain the eigenvalues, we can look for the zeros of the characteristic polynomial  $\det(T - \lambda I)$ , with  $I$  the identity matrix. A direct calculation shows that

$$\det(T - \lambda I) = \lambda^2 + 1 - \frac{\lambda}{t} [(t^2 - r^2)e^{-i\beta a} + e^{+i\beta a}]. \quad (18)$$

Next we note that  $t^2 - r^2 = t + r$ , but also that

$$\lambda + \frac{1}{\lambda} = 2\cos(ka). \quad (19)$$

We thus get the dispersion relation

$$\cos(ka) = \cos(\beta a) + i\frac{r}{t}\sin(\beta a). \quad (20)$$

A smooth dependence with frequency enters via the definition of  $\beta$ , but a sharp dependence around the resonance frequency enters via  $r$  and  $t$ . Formula (20) is different from equation (S1) in the supplementary information of [17] in that it explicitly takes reflection into account. It also models both Bragg and LR band gaps, as we illustrate later.

To understand the physical meaning of this dispersion relation, let us first remark that whenever reflection is negligible ( $r = 0$ ), transmission is unity ( $t = 1$ ) and the dispersion relation reduces to  $k = \pm\beta$ . Physically, the waves propagating along the waveguide do not see the local resonator and nothing particular happens. Now, as we approach resonance,  $t$  becomes smaller and  $r$  increases. As a result, the second term ( $\sin(\beta a)$ ) will dominate over the first one ( $\cos(\beta a)$ ) as resonance is approached. It is actually useful to express

$$\frac{r}{t} = \frac{t - 1}{t} = iL(\omega) \frac{2\alpha\kappa_{11} + L(\omega)(\kappa_{11}\kappa_{22} - \kappa_{12}\kappa_{21})}{2\beta(2\alpha + L(\omega)\kappa_{22})}. \quad (21)$$

Finally, we can express the dispersion relation as

$$\begin{aligned} \cos(ka) &= \cos(\omega a / c) \\ &- L(\omega) \frac{2\alpha\kappa_{11} + L(\omega)(\kappa_{11}\kappa_{22} - \kappa_{12}\kappa_{21})}{2\beta(2\alpha + L(\omega)\kappa_{22})} \sin(\omega a / c). \end{aligned} \quad (22)$$

In the absence of loss,  $L(\omega)$  is purely real. Assuming further that the coupling constants  $\kappa_{ij}$  are real, the right-hand side is real also. The resonant term in factor of  $\sin(\beta a)$  goes to  $\pm\infty$  at frequency  $\omega_0$ . Around the resonant frequency, there is a range of frequencies where  $k$  becomes complex, defined by the condition  $|\cos(ka)| > 1$ . A band gap is thus introduced by the periodic array of resonators grafted on the waveguide.

The complex band structures predicted by this theory are presented in figures 5 and 6. They are plotted with exactly the same parameters as used in figure 4, i.e. they are fitted from the single resonator case. The complex band structures obtained from the model are found to be in excellent agreement with the FEM results in the long lattice constant case. Inside the

LR band gap of figure 5(a), the real part of the wavenumber reaches 0 at the LR band gap entrance, stays constant until the resonant frequency 1459.7 Hz where it suddenly flips to  $\pi/a$ , reflecting a sign change as the resonance is crossed. Meanwhile, the imaginary part of the wavenumber increases from zero at the LR band gap entrance to a sharp maximum at the resonant frequency, before dropping again to zero at the LR band gap exit, forming a cusp. One may also notice that in figure 5(a), the theoretical model also predicts very well the Bragg band gap below the local resonance. Even if the reflection on the resonator is small at this frequency according to figure 4(a), it can still produce  $|\cos(ka)| > 1$ .

As compared to a full-fledged FEM numerical simulation, which includes all possible waves, the model of the complex band structure that we have devised in this section only operates on the propagating guided waves. The evanescent guided waves attached to the grafting points are still included, of course, via the reflection and transmission coefficients  $r$  and  $t$ , but any possible evanescent coupling between resonators is not included. While the model predicts quite accurately the features of the long lattice measurements, significant deviations are found, especially at high frequencies, in figure 6 in the short lattice case. The model for instance fails to predict the shift of the resonant frequency observed experimentally in figure 6(a). The FEM complex band structure (for an infinite period crystal) is also in very good agreement with measurements (for a periodic sequence of five resonators) in the long lattice constant case, but disagrees even more than the model in the short lattice case. These results suggest that the commonly implied assumption that the resonators can always be considered to be decoupled may not hold for all LR phononic crystals. Such evanescent coupling between resonators could seriously impair the band gap properties of strongly sub-wavelength LR phononic crystals, e.g. if the distance between resonators is decreased below a value related to the spatial extent of evanescent waves attached to the grafting points.

## 6. Conclusion

We have investigated the band gap properties of a system containing a single or a periodic array of resonators grafted onto the waveguide via experiment, theory and numerical simulation. The LR band gaps were found to be very sensitive to the lattice constant. When a single resonator is grafted onto the waveguide, transmission dips are observed at frequencies different from the natural frequencies of the resonator. A theoretical model considering the coupling of the evanescent and propagating guided waves was developed to explain this transmission cancelling phenomenon and the frequency shift. Both the theoretical and the simulated results are in good agreement with the experimental results.

When a finite number of resonators are grafted periodically along the waveguide, band gaps appear at the resonant frequencies. In the long lattice constant case, the complex band structure predicted by the theoretical model is in good agreement with the simulated results obtained with FEM. Significantly, it

is found that the difference between Bragg and LR band gaps can be told by observing the shape of the complex band structure and that the latter can be modelled with a simple explicit formula. This observation was confirmed by the experimental results in the long lattice constant regime.

When the lattice constant becomes small enough (e.g. when it becomes sub-wavelength), the interference between resonators is probably strong enough that it cannot be neglected anymore. We found numerically that the LR band gap can even be almost cancelled. The theoretical model we proposed does not consider the interference between resonators and does not explain well the experimental observations. Further investigation of the resilience of LR band gaps when the lattice constant becomes strongly sub-wavelength is required.

## Acknowledgments

The authors would like to thank Dr Sarah Benchabane for help in carrying out the experiment and for fruitful discussion. Financial support by the Labex ACTION program (Contract No. ANR-11-LABX-01-01) is gratefully acknowledged. The first and the third authors are grateful to the support from the National Natural Science Foundation of China (11302021). The first author also thanks the Visiting Fund of Beijing Jiaotong University for supporting his visit to Besancon.

## References

- [1] Kushwaha M S, Halevi P, Dobrzynski L and Djafari-Rouhani B 1993 *Phys. Rev. Lett.* **71** 2022
- [2] Liu Z, Zhang X, Mao Y, Zhu Y Y, Yang Z, Chan C T and Sheng P 2000 *Science* **289** 1734
- [3] Benchabane S, Khelif A, Choujaa A, Djafari-Rouhani B and Laude V 2005 *Europhys. Lett.* **71** 570
- [4] Sainidou R, Djafari-Rouhani B, Pennec Y and Vasseur J O 2006 *Phys. Rev. B* **73** 024302
- [5] Achaoui Y, Khelif A, Benchabane S, Robert L and Laude V 2011 *Phys. Rev. B* **83** 104201
- [6] Lemoult F, Fink M and Lerosey G 2011 *Phys. Rev. Lett.* **107** 064301
- [7] Richoux O, Tournat V and Le Van Suu T 2007 *Phys. Rev. E* **75** 026615
- [8] Kushwaha M S, Akjouj A, Djafari-Rouhani B, Dobrzynski L and Vasseur J O 1998 *Solid State Commun.* **106** 659
- [9] Potel C and Bruneau M 2006 *Acoustique Générale* (Paris: Ellipses). Animations of the first acoustic modes of cylindrical waveguides are available at [http://perso.univ-lemans.fr/~cpotel/stationary\\_modes\\_infinite\\_cylinder\\_gb.html](http://perso.univ-lemans.fr/~cpotel/stationary_modes_infinite_cylinder_gb.html)
- [10] Fang N, Xi D, Xu J, Ambati M, Srituravanich W, Sun C and Zhang X 2006 *Nat. Mater.* **5** 452
- [11] Christensen J, Martin-Moreno L and Garcia-Vidal F J 2008 *Phys. Rev. Lett.* **101** 014301
- [12] Joe Y S, Satanin A M and Kim C S 2006 *Phys. Scr.* **74** 259
- [13] Achenbach J D 1973 *Wave Propagation in Elastic Solids* (London: North Holland)
- [14] Laude V, Moiseyenko R P, Benchabane S and Declercq N 2011 *AIP Adv.* **1** 041402
- [15] Bradley C E 1994 *J. Acoust. Soc. Am.* **96** 1844
- [16] Sugimoto N and Horioka T 1995 *J. Acoust. Soc. Am.* **97** 1446
- [17] Lemoult F, Kaina N, Fink M and Lerosey G 2013 *Nat. Phys.* **9** 55